2024 IEEE/RSJ International Conference on Intelligent Robots and Systems (IROS)
October 14-18, 2024. Abu Dhabi, UAE

Modeling and Analysis of Passive Quadruped Walker with Compliant Torso on Low-friction Surface

Yuxuan Xiang[1], Yanqiu Zheng[2] and Fumihiko Asano[1]

***Abstract*— The quadrupeds have wider active territory than humans. Their bodies can adapt various environments through evolution, enabling the efficient, elegant gait for their legged locomotion. Previous researches have indicated lots of examples of utilizing the advantages of body to achieve environment adaptive and stable gait, and for legged locomotion, especially with quadruped robot determining how to generate environment-adaptive mobile locomotion remains a significant challenge. In this study, we discussed the adaptability to environments of quadruped robots, specific walking stability and gait convergence in low-friction environments with compliant torso. The numerically simulations are proposed for observing the trend of walking performance with various friction coefficient. By analyzing the typical walking gait, the adaptability of quadruped walkers with compliant torso are found. These conclusions contribute to the design and development of compliant torso for quadruped walkers.**

I. INTRODUCTION

In the nature world, the most quadrupeds live in the complex environment, and had wider active territory than humans. They can effectively locomote through various challenging areas, including forests, cliffs and deserts. For example, camels can walk in the desert efficiently, antelopes can move swiftly over the cliffs, and polar bears can crawl steadily on ice. They have compliant bodies and developed corresponding motion behaviors to adapt environments through evolution. Benefit from these advantages, quadrupeds demonstrate exceptional mobility and performance in various environments.

Through the studies of biomechanical, a biological spine is composed of rigid structures and flexible tissues [1], [2], which can maintain dynamic balance and possesses robustness within a certain range. As same as the biological spine, the tensegrity structures are also combined by rigid components and soft cables, demonstrated excellent compliance [3], [4]. The past researches has exhibited the robustness and practicality of the spine with tensegrity structures. In summary, the structures consisted by rigid and elastic component can effectively illustrate compliance.

On the other hands, by studying the motion mechanisms of quadrupeds, the quadruped robots with rigid torso, equipped with terrain sensors, advanced actuators, and dynamic controls, shown excellent adaptability on rough terrains, and had greatly contributed to the field of legged mobile robotics [5], [6]. In the studies of gait analysis of quadruped robots, however, the robot with rigid torso can only exhibit partial compliance, offer limited reference for the generation of adaptive gaits. Robots like Cheetah-cub and Lynx-robot have had their locomotion performance improved by increasing the compliance of their spines [7]–[9]. Furthermore, the influence of tensegrity structure as compliance torso on gait adaptability in quadruped robots has not been widely discussed. In this paper, to enhance the environmental adaptability of quadruped robot's gait, a combination of rigid and elastic element structures called compliant torso is proposed. As the improvement of past rigid torso, the compliant torso has the advantages of absorbing impacts and storing energy.

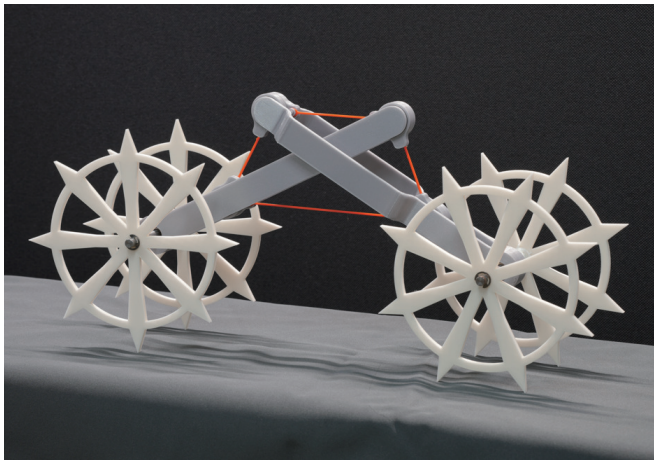

Fig. 1. Prototype of passive quadruped walker with compliant torso. The orange elastic element and grey frame are made by 3D-print using TPU and PLA materials, respectively.

Moreover, by recognizing that the walking of quadrupeds is the inverted pendulum-like motion generated by forelimbs and hindlimbs, respectively [10]–[12]. Consequently, we used the rimless wheel, which is capable of producing typical inverted pendulum motion, to represent the forelimbs and hindlimbs of quadrupeds. As shown in Fig. 1 the prototype for experiment, two rimless wheels are connected utilizing the compliant torso (combination of grey frame and orange elastic element) to form a quadruped walker.

Additionaly, passive walking was proposed by McGeer in 1990 [13] which can generate the human-like gait without any actuation, only relying on the conversion between gravitational potential energy and kinetic energy [14], [15]. Conclusively, the structure will greatly determine the dynamics

This research was partially supported by Grant-in-Aid for Scientific Research (C) No. 23K03727, provided by the Japan Society for the Promotion of Science (JSPS).

[1]Yuxuan Xiang and Fumihiko Asano are with the Graduate School of Advanced Science and Technology, Japan Advanced Institute of Science and Technology, 1-1 Asahidai, Nomi, Ishikawa 923-1292, Japan {kouuken,fasano}@jaist.ac.jp

[2]Yanqiu Zheng is with the Department of Mechanical Engineering, Ritsumeikan University, 1-1-1 Nojihigashi, Kusatsu Shiga 525-8577, Japan zhengyq@fc.ritsumei.ac.jp

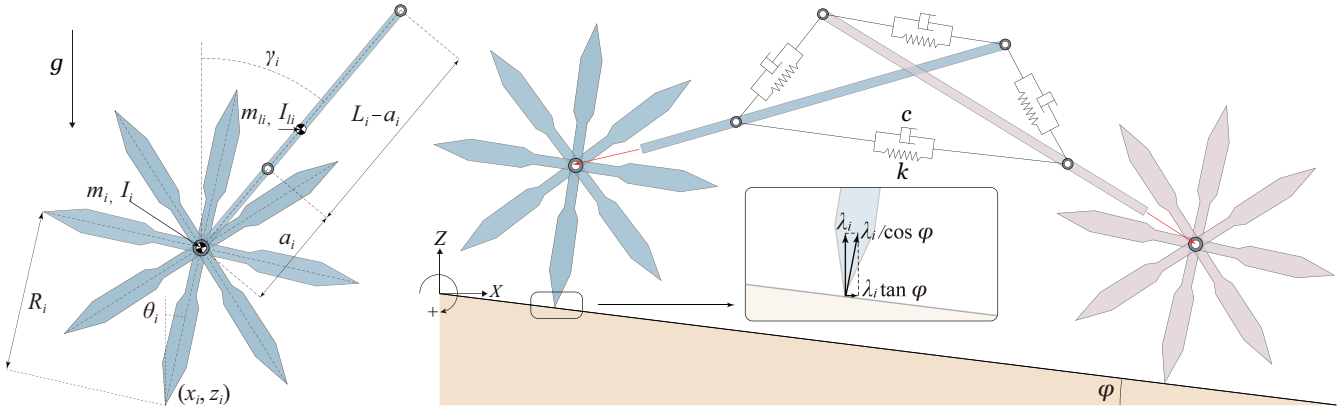

(a) Coordinate system for rimless wheel with upper torso

(b) Passive quadruped walker walking on low-friction downhill surface

Fig. 2. Mathematical model of passive quadruped walker with compliant torso

characteristics of itself. It is expected to use passive walking as a method to demonstrate the motion characteristics of the passive quadruped walker with compliant torso.

In this paper, as the foundational research for designing compliant torso of quadruped robots, the authors proposed a model of compliant torso a combination of rigid limb and elastic element. To disscuss the influence of compliant torso on environment-adaptive gait, the simulator is developed to investigate the capability of adapt to environments of the model, especially on low-friction surface. The simulation results show the quadruped walker with compliant torso could achieve stable passive walking and phase convergence on the low-friction surface. By comparing the walking performance of quadruped walker with rigid and compliant torso, the adaptive of the compliant body is demonstrated.

II. MODELING

A. Model Assumptions

In this study, the model proposed consists two rimless wheels with their upper limb connected by elastic elements. The combination of upper limbs can be seen as a compliant torso. Additionally, due to rimless wheel has capability of generating the inverted pendulum motion, therefore, it is used to represent the forelimb and hindlimb of quadruped. Fig. 2 (a) illustrates the system's coordinates and the physical parameters of the model, the specific configuration are :

- The (x_i, z_i) represents the location of ground contact points of the i_{th} rimless wheel. θ_i denotes the angle position of the i_{th} rimless wheel relative to the vertical.
- Since rimless wheel includes eight identical limbs, the angle between each limb is $\pi/4$ [rad]. R_i is the length of the limb, and m_i and I_i indicate the mass and inertia moment of the rimless wheel, respectively.
- The upper limb is attached to the center of the rimless wheel through passive rotation joints, with a rotation angle position relative to the vertical denoted by γ_i. The center of mass of upper limb is located in the middle of it, denoted by mass m_{li} with the inertia moment I_{li}.
- Two upper limbs are interconnected by elastic elements, forming a compliant torso. The locations of the elastic element connection point on the upper limbs are described by a_i, representing the distance from the passive rotation joint on the rimless wheel to the first elastic element connection point. Due to another connection point is set on the other side of upper limb, and the length of upper limb is L_i, the distance between two connection point is $L_i - a_i$.

Additionally, the subscripts i represent the rimless wheel mark, that is, $i \in \{1,2\}$, with "1" and "2" specifically indicating the front and rear wheels, respectively.

B. Equation of Motion

The generalized coordinates vector can be denoted as: $\boldsymbol{q} = \begin{bmatrix} x_1 & z_1 & \theta_1 & \gamma_1 & x_2 & z_2 & \theta_2 & \gamma_2 \end{bmatrix}^{\mathrm{T}}$, the equation of motion and holonomic constraint condition of system can be described as follows:

$$\boldsymbol{M}\ddot{\boldsymbol{q}} + \boldsymbol{h} = \boldsymbol{J}_c^{\mathrm{T}}\boldsymbol{\lambda}_c + \boldsymbol{J}_\mu^{\mathrm{T}}\boldsymbol{\lambda}_c + \boldsymbol{J}_T^{\mathrm{T}}\boldsymbol{T}, \tag{1}$$

$$\boldsymbol{J}_c\dot{\boldsymbol{q}} = \boldsymbol{0}_{2\times 1}, \tag{2}$$

where $\boldsymbol{M}$ represents the inertia matrix, $\boldsymbol{h}$ including the central force, coriolis force, and gravity terms. On the right side of Eq. (1), $\boldsymbol{J}_c^{\mathrm{T}}\boldsymbol{\lambda}_c$ is the holonomic constraint, $\boldsymbol{J}_\mu^{\mathrm{T}}\boldsymbol{\lambda}_c$ is the friction force and $\boldsymbol{J}_T^{\mathrm{T}}\boldsymbol{T}$ is the tension due to elastic element.

Additionally, as represented by Eq. (2), it is assumed that quadruped walker locomotes in the low-friction environment, meaning the surface is slippery, and both front and the rear rimless wheel have a limb in contact with the ground. Therefore the velocity constraint equation are shown as follows:

$$\dot{z}_1 = -\dot{x}_1 \tan\varphi, \quad \dot{z}_2 = -\dot{x}_2 \tan\varphi. \tag{3}$$

By summarizing Eq. (3), The constraint Jacobian matrix $\boldsymbol{J}_c$ can be obtained as:

$$\boldsymbol{J}_c = \begin{bmatrix} \tan\varphi & 1 & 0 & 0 & 0 & 0 & 0 & 0 \\ 0 & 0 & 0 & 0 & \tan\varphi & 1 & 0 & 0 \end{bmatrix}. \tag{4}$$

The time derivative of Eq. (2) becomes:

$$\boldsymbol{J}_c\ddot{\boldsymbol{q}} = \boldsymbol{0}_{2\times 1}, \tag{5}$$

given that the forelimb and hindlimb are in contact with the ground separately, therefore $\boldsymbol{\lambda}_c = \begin{bmatrix}\lambda_1 \lambda_2\end{bmatrix}^{\mathrm{T}}$, and by solving Eq. (5) and Eq. (1), $\boldsymbol{\lambda}_c \in \mathbb{R}^2$ can be obtained as:

$$\boldsymbol{\lambda}_c = -\boldsymbol{X}^{-1}\boldsymbol{J}_c\boldsymbol{M}^{-1}(\boldsymbol{J}_T^{\mathrm{T}}\boldsymbol{T} - \boldsymbol{h}), \tag{6}$$

$$\boldsymbol{X} = \boldsymbol{J}_c\boldsymbol{M}^{-1}(\boldsymbol{J}_c^{\mathrm{T}} + \boldsymbol{J}_\mu^{\mathrm{T}}). \tag{7}$$

C. Coulomb Friction Force

In this study, to clarify the locomotion performance of the quadruped walker on slippery surfaces and thereby to observe the model's adaptability to low-friction environments, the Coulomb friction model used to calculate the frictional forces acting on the system. The f is used to represent the frictional force applied at the ground contact points, and f can be specified by geometric relationships:

$$f = \mu\frac{\lambda_i}{\cos\varphi}, \tag{8}$$

where λ_i is the constraint force shown as Fig. 2 (b), μ is the signed friction coefficient determined by the velocity of contact point is calculated as:

$$\mu = -\mu_0 \tanh(\varepsilon v). \tag{9}$$

In Eq. (9), ε is a dimensionless parameter that adjusts the slope of μ around $v = 0$, where the sliding velocity to the stationary surface v is specified as:

$$v = \frac{\dot{x}_i}{\cos\varphi}. \tag{10}$$

For each limb, the friction force vector is:

$$\begin{bmatrix}\cos\varphi \\ -\sin\varphi \\ 0 \\ 0\end{bmatrix} f = \begin{bmatrix}\mu \\ -\mu\tan\varphi \\ 0 \\ 0\end{bmatrix}\lambda_i, \tag{11}$$

consequently, the $\boldsymbol{J}_\mu^{\mathrm{T}}\boldsymbol{\lambda}_c$ in the Eq. (1) can be descried as:

$$\boldsymbol{J}_\mu^{\mathrm{T}}\boldsymbol{\lambda}_c = \begin{bmatrix}\mu & -\mu\tan\varphi & 0 & 0 & 0 & 0 & 0 & 0 \\ 0 & 0 & 0 & 0 & \mu & -\mu\tan\varphi & 0 & 0\end{bmatrix}^{\mathrm{T}}\boldsymbol{\lambda}_c. \tag{12}$$

D. Tension

Fig. 3 shows the connection details of the elastic elements. Each connection point subjected tension from two different directions on upper limb, the model has total four connection points, the specific tension force vector can be calculated as:

$$\boldsymbol{J}_T^{\mathrm{T}}\boldsymbol{T} = \begin{bmatrix}\boldsymbol{J}_1^{\mathrm{T}} \boldsymbol{J}_2^{\mathrm{T}} \dots \dots \boldsymbol{J}_7^{\mathrm{T}} \boldsymbol{J}_8^{\mathrm{T}}\end{bmatrix}\begin{bmatrix}T_1 \\ T_2 \\ \cdots \\ \cdots \\ T_7 \\ T_8\end{bmatrix}. \tag{13}$$

The tension of the whole system consisted of 4 elastic elements, and the connection order is: $A \to B$, $B \to C$, $C \to D$ and $D \to A$. We take an element from matrix (13) as a example: $\boldsymbol{J}_1^{\mathrm{T}}\boldsymbol{T}_1$ represents the tension applied at point A (marked with red color from Fig. 13), and its tension can be described as:

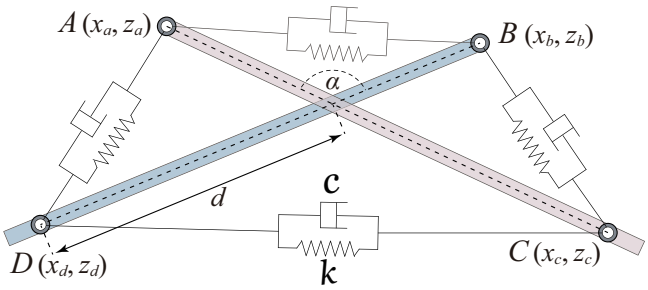

Fig. 3. The detail of compliant torso. In this figure, α is the angle between the upper limb, d is the distance between the connection point of elastic element to the intersection point of upper limbs.

$$\boldsymbol{J}_1^{\mathrm{T}}\boldsymbol{T}_1 = \boldsymbol{J}_{AB}^{\mathrm{T}}T_{AB}, \tag{14}$$

where $\boldsymbol{J}_{AB}$ is the Jacobain vector of connection point A on upper limb of fore rimless wheel. The $\boldsymbol{d}_{AB}$ represents the direction vector from connection point $A \to B$. The details are shown as follows:

$$\boldsymbol{J}_{AB} = \begin{bmatrix}0\,0\,0\,0\,1\,0 & R_2\cos\theta_2 & L_2\cos\gamma_2 \\ 0\,0\,0\,0\,0\,1 & -R_2\sin\theta_2 & -L_2\sin\gamma_2\end{bmatrix}, \tag{15}$$

$$\boldsymbol{d}_{AB} = \boldsymbol{P}_{AB}/D_{AB}, \tag{16}$$

here, (x_a, z_a) to (x_b, z_b) represents the coordinate of connection point A and B, respectively, so the displacement vector and distance can be obtained as:

$$\boldsymbol{P}_{AB} := \begin{bmatrix}x_b - x_a \\ z_b - z_a\end{bmatrix}, \quad \boldsymbol{V}_{AB} := \begin{bmatrix}\dot{x}_b - \dot{x}_a \\ \dot{z}_b - \dot{z}_a\end{bmatrix}, \tag{17}$$

$$D_{AB} := \sqrt{(x_b - x_a)^2 + (z_b - z_a)^2}, \tag{18}$$

$$T_{AB} = k(D_{AB} - l_n) + c\boldsymbol{V}_{AB}^{\mathrm{T}}\boldsymbol{d}_{AB}, \tag{19}$$

where k [N/m] and c [N·s/m] are stiffness and viscosity coefficient of elastic element, respectively. l_n [m] is the nature length of the elastic element.

E. Collision Equation

It is assumed that when the next limb of rimless wheels impact to the ground, the limb in contact will leave the ground immediately according to the inelastic collision model. The holonomic constraint equation after impact can be formulated as follow:

$$\boldsymbol{M}\dot{\boldsymbol{q}}^+ = \boldsymbol{M}\dot{\boldsymbol{q}}^- + \boldsymbol{J}_I^{\mathrm{T}}\boldsymbol{\lambda}_I \tag{20}$$

$$\boldsymbol{J}_I\dot{\boldsymbol{q}}^+ = \boldsymbol{0}_{2\times 1} \tag{21}$$

the superscripts "$-$" and "$+$" denote immediately before and immediately after impact, respectively. The $\boldsymbol{J}_I$ is the Jacobian vector of constrain force at collision, then the constrained condition is:

$$\dot{x}_I^+ = 0, \quad \dot{z}_I^+ = 0, \tag{22}$$

and can be further arranged as follows:

$$\boldsymbol{J}_I\dot{\boldsymbol{q}}^+ = \begin{bmatrix} 1\,0 & R_f\cos(\theta_f+3\pi/4) & 0\,0\,0\,0\,0 \\ 0\,1 & -R_f\sin(\theta_f+3\pi/4) & 0\,0\,0\,0\,0 \end{bmatrix}\dot{\boldsymbol{q}}^+ = \boldsymbol{0}. \quad (23)$$

By solving Eq. (20) and (21) , the Lagrange multiplier vector $\boldsymbol{\lambda}_I$ can be derived as:

$$\boldsymbol{\lambda}_I = -\boldsymbol{X}_I^{-1}\boldsymbol{J}_I\dot{\boldsymbol{q}}^-, \boldsymbol{X}_I = \boldsymbol{J}_I\boldsymbol{M}^{-1}\boldsymbol{J}_I^{\mathrm{T}}. \quad (24)$$

The velocity vector immediately after impact can be obtained as:

$$\dot{\boldsymbol{q}}^+ = \left(\boldsymbol{I}_8 - \boldsymbol{M}^{-1}\boldsymbol{J}_I^{\mathrm{T}}\boldsymbol{X}_I^{-1}\boldsymbol{J}_I\right)\dot{\boldsymbol{q}}^-. \quad (25)$$

III. GAIT ANALYSIS

A. Walking gait generation

In this section, aiming that to explore the walking performance of quadruped walkers with compliant torso on low-friction surfaces, the numerical simulator of the quadruped walker's passive walking on downhill with friction is developed. It is set up the simulation time for 60 seconds and only take the simulation result of last 20 steps. Under the same condition, if the simulation results overlap into a same point, that indicates the walking gaits have converged, we consider this as stable. Conversely, if the simulation results do not overlap but scattered, that indicates the walking gaits lack of convergence, and we consider this as unstable. This approach is enable to effectively determine the stability of the walking gait and also can observe the walking performance after the gait has stabilized. The initial state of robot started passive dynamic walking as shown in matrix (26):

$$\boldsymbol{q}(0) = \begin{bmatrix} 0 \\ 0 \\ 0 \\ \varphi + \frac{\alpha}{2} \\ 2d\cos\varphi\sin\frac{\alpha}{2} \\ -2d\sin\varphi\sin\frac{\alpha}{2} \\ \pi/16 \\ \varphi - \frac{\alpha}{2} \end{bmatrix}, \quad \dot{\boldsymbol{q}}(0) = \begin{bmatrix} 0 \\ 0 \\ 3 \\ 0 \\ 0 \\ 0 \\ 3 \\ 0 \end{bmatrix} \quad (26)$$

Due to the connection between forelimb and hindlimb has elasticity and compliant, which can absorb the impact and store energy, it is expected that energy-efficient and adaptive walking gait can be generated successfully.

TABLE I
PHYSICAL PARAMETERS OF SYSTEM

Symbol	Value	Unit	Symbol	Value	Unit
$m_1 = m_2$	0.1	kg	g	9.81	m/s^2
$I_1 = I_2$	0.0005	kg·m^2	k	150	N·m
$R_1 = R_2$	0.1	m	c	5	N·s/m
$m_{l1} = m_{l2}$	0.1	kg	d	0.0525	m
$I_{l1} = I_{l2}$	0.0016	kg·m^2	α	125	deg
$L_1 = L_2$	0.25	m	$a_1 = a_2$	0.08	m

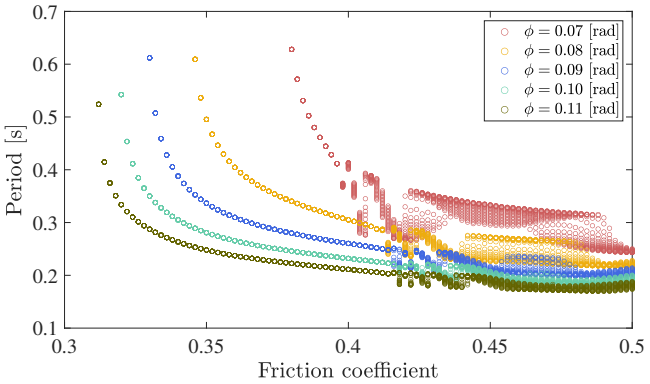

(a) Period versus friction coefficient

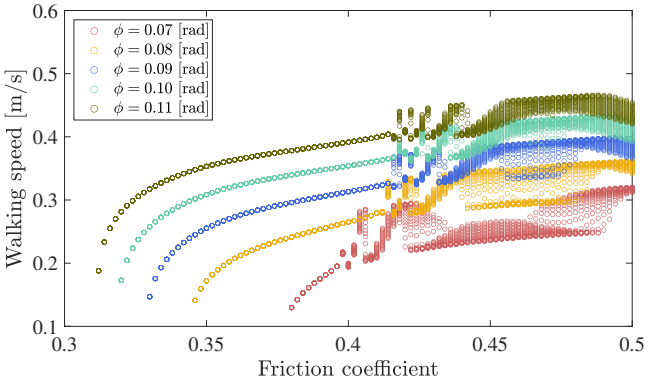

(b) Walking speed versus friction coefficient

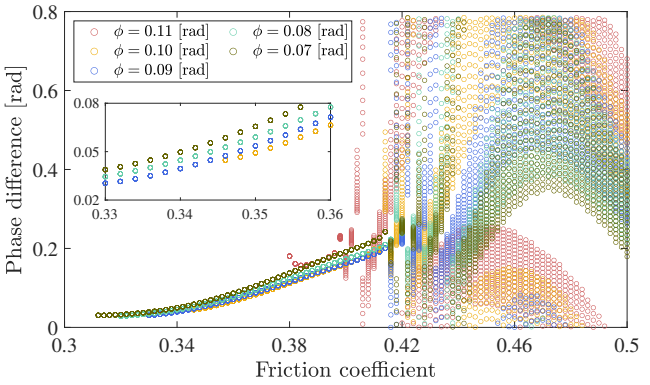

(c) Phase difference versus friction coefficient

Fig. 4. Simulation results of walking performance versus variable friction coefficient μ under five value of downhill angle φ [rad]

B. Motion analysis

Fig. 4 demonstrates the walking performance of passive quadruped walker with compliant torso for variable friction coefficient μ, under five values of downhill angle conditions φ. The physical parameters are chosen as the same values as listed in Table I.

Fig. 4 (a),(b) show the period and walking speed of walking performance, respectively, when the friction coefficient $\mu > 0.3$, the quadruped walker begins to exhibit a stable 1-period gait, and as the friction coefficient increases, the period gradually becomes shorter. At approximately μ=0.4, multi-period gaits and chaotic period start to occur, indicating that the gait becomes unstable. The colors marked in the figure represent simulation results under different

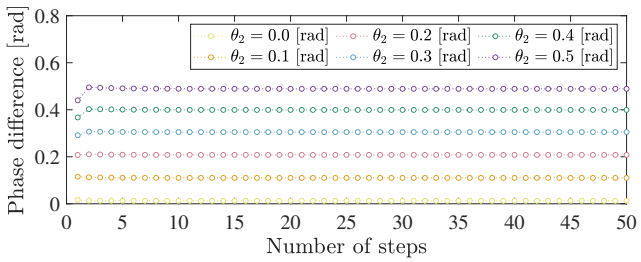

(a) Phase difference versus number of steps

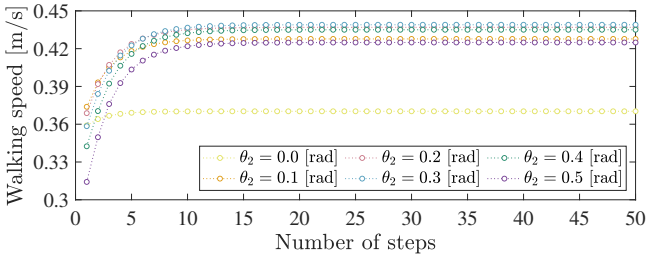

(b) Walking speed versus number of steps

Fig. 5. Walking performance evaluation of quadruped walker with compliant torso during 50 steps with different initial phase difference on the non-friction environment

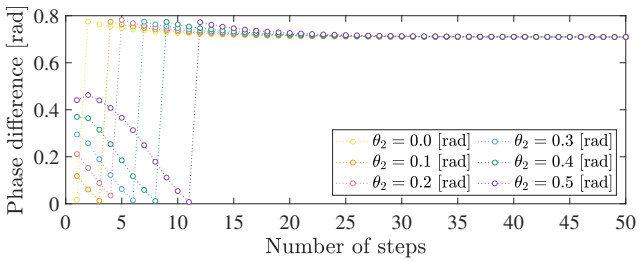

(a) Phase difference versus number of steps

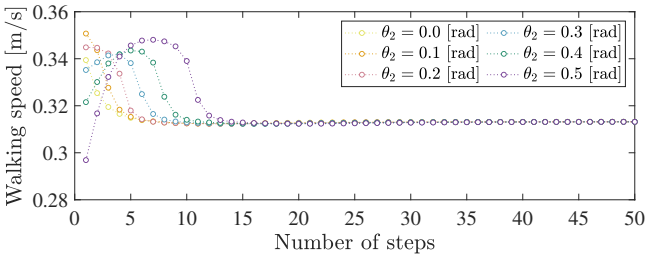

(b) Walking speed versus number of steps

Fig. 6. Walking performance evaluation of quadruped walker with compliant torso during 50 steps with different initial phase difference on the low-friction surface where μ=0.35 and φ=0.08 [rad]

downhill conditions with φ. It is observed that in low-friction environment, the stable 1-period gait is generated more easily on the steeper downhill. Moreover, for the same friction coefficient, a steeper downhill corresponds to a shorter period, meaning the faster walking speed. Since the passive quadruped walker has forelimb and hindlimb, the Fig. 4(c) specifically shows the phase difference between forelimb and hindlimb. By comparing Fig. 4 (a),(b) and (c), it is found that under low friction coefficient, when the walking speed become stabilized, the phase difference between the front and rear wheels is consistent. For system stability, it is unclear whether a consistent speed and phase difference are a couple of necessary and sufficient condition. The author think, however, it is indicated that adjusting the phase difference between the forelimb and hindlimb can lead to stabilization of the system.

C. Analysis of typical walking gait

In this section, to further investigate the influence of phase difference effect on walking performance especially stability, it is analyzed the typical gaits extracted from Fig. 4 and examined the stability of motion performance under the same conditions, but in different environments: non-friction, low-friction and high-friction. Additionally, it is also compared the walking gait of quadruped walker with rigid torso in the low-friction environment.

First, the typical walking gait in the non-friction environment is analyzed by numerical simulation as shown in Fig. 5. Due to the initial value of θ_1 is set to 0 [rad], the initial value of θ_2 can represent initial phase difference between forelimb and hindlimb. From fig. 5(a), it is obviously to obserbed that in the non-friction environment, the initial phase difference is the phase difference when the walking gait become stable. In fig. 5(b), we can find that with initial phase difference, the passive quadruped walker can generate stable walking

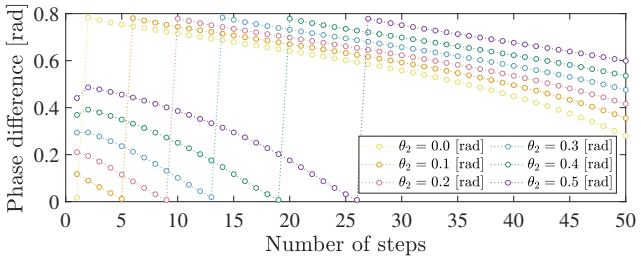

(a) Phase difference versus number of steps

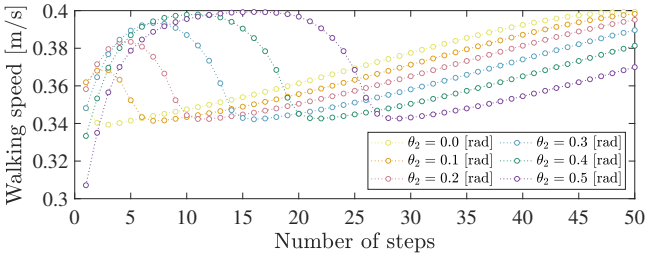

(b) Walking speed versus number of steps

Fig. 7. Walking performance evaluation of quadruped walker with compliant torso during 50 steps with different initial phase difference on the low-friction surface where μ=0.5 and φ=0.08 [rad]

gait but different walking performance. It is investigated that walking performance is effected by the initial conditions. Fig. 6 shows the simulation results during 50 steps with different initial phase difference on the low-friction surface where μ=0.35 and φ=0.08 [rad]. We can found that despite the initial phase differences are not consistent, after 15 steps of passive walking in a low-friction environment, the walking gait become stable, and the phase difference between forelimb and hindlimb also converges to a consistent value.

Fig. 7 shows the typical walking gait in the high-friction environment where μ=0.5. Compared to the gait in low-friction environment, even after 50 steps of passive walking

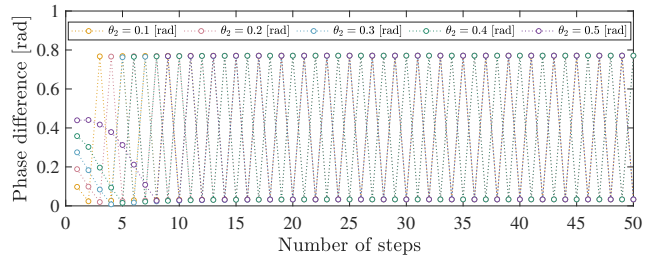

(a) Phase difference versus number of steps

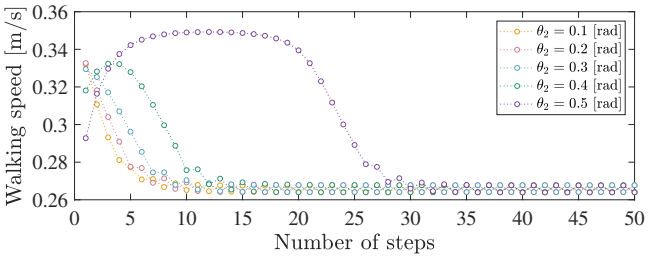

(b) Walking speed versus number of steps

Fig. 8. Walking performance evaluation of quadruped walker with rigid torso during 50 steps with different initial phase difference on the lowfriction surface

the walking gait remain unstable, and the phase difference fails to converge.

To compare the walking stability of rigid and compliant torsos in friction environments, Fig. 8 displays the simulation results for the passive quadruped walker with a rigid torso, which is described as a combination of two rimless wheel connected by a rigid rod. From Fig. 8, we can find that passive quadruped walker with a rigid torso generated 2-period gait, but the phase difference still can not converge to a consistent value. Therefore, the author suggests that the the quadruped walker with compliant torso exhibits better walking stability in low-friction environments.

IV. DISCUSSION

The passive quadruped walker with a compliant torso can achieve stable dynamic walking on a gentle slope. Under the low-friction environments, the compliant torso can provide the capability of adjusting phase difference between forelimb and hindlimb. The author believe that the compliant torso can actively utilizing the friction to improve the walking stability by aligning the phase differences, but further validation is needed. By comparing the walking performance of passive quadruped walkers with rigid and compliant torsos on low-friction surfaces, we observed better convergence in the case of compliant torso. This suggests that a compliant torso offers stronger adaptability to the environment. Furthermore, the additional advantages of a compliant torso are worthy to explore and research further.

V. CONCLUSION AND FUTURE WORK

This study proposed a dynamic model of passive quadruped walkers with compliant torso on slippery road surface. It is found that the quadruped walkers with compliant torsos can generate stable passive walking gaits on low-friction environments. The influence of compliant torso on the environmental adaptability of passive quadruped walkers on low-friction environments are discussed, Specifically, by observing walking performance under various friction coefficients. It is revealed the phenomenon of phase convergence between forelimb and hindlimb with different initial conditions by analyzing the different typical gaits on low-friction environments. Moreover, by comparing the walking performances of rigid and compliant torsos, the potential advantages of compliant torsos in adapting to the environment is demonstrated, which can contribute to the design and optimization of quadrupedal walkers.

In the future, we will continue to explore the advantages of compliant torsos and verify the feasibility and effectiveness through experiments. In specific applications, we aim to utilize the benefits of compliant torso for to achieve greater environmental adaptability locomotion modes.

REFERENCES

[1] R. J. Kowalski, L. A. Ferrara, and E. C. Benzel, "Biomechanics of the spine," *Neurosurgery Quarterly*, vol. 15, pp. 42–59, 2005.

[2] S. Levin, "The tensegrity-truss as a model for spine mechanics: Biotenseglrity," *Journal of Mechanics in Medicine and Biology*, vol. 02, 2011.

[3] C. Paul, F. Valero-Cuevas, and H. Lipson, "Design and control of tensegrity robots for locomotion," *IEEE Transactions on Robotics*, vol. 22, no. 5, pp. 944–957, 2006.

[4] A. P. Sabelhaus, J. Bruce, K. Caluwaerts, P. Manovi, R. F. Firoozi, S. Dobi, A. M. Agogino, and V. SunSpiral, "System design and locomotion of superball, an untethered tensegrity robot," *2015 IEEE International Conference on Robotics and Automation*, pp. 2867–2873, 2015.

[5] M. Raibert, K. Blankespoor, G. Nelson, and R. Playter, "Bigdog, the rough-terrain quadruped robot," *IFAC Proceedings Volumes*, vol. 41, no. 2, pp. 10 822–10 825, 2008, 17th IFAC World Congress.

[6] D. Wooden, M. Malchano, K. Blankespoor, A. Howardy, A. A. Rizzi, and M. Raibert, "Autonomous navigation for bigdog," in *IEEE International Conference on Robotics and Automation*, 2010, pp. 4736–4741.

[7] A. Badri-Spröwitz, A. Tuleu, M. Vespignani, M. Ajallooeian, E. Badri, and A. Ijspeert, "Towards dynamic trot gait locomotion: Design, control, and experiments with cheetah-cub, a compliant quadruped robot," *The International Journal of Robotics Research*, vol. 32, 07 2013.

[8] M. Khoramshahi, A. Spröwitz, A. Tuleu, M. N. Ahmadabadi, and A. J. Ijspeert, "Benefits of an active spine supported bounding locomotion with a small compliant quadruped robot," in *2013 IEEE International Conference on Robotics and Automation*, 2013, pp. 3329–3334.

[9] P. Eckert, A. Spröwitz, H. Witte, and A. J. Ijspeert, "Comparing the effect of different spine and leg designs for a small bounding quadruped robot," in *2015 IEEE International Conference on Robotics and Automation*, 2015, pp. 3128–3133.

[10] R. M. Alexander and A. Jayes, "Optimum walking techniques for idealized animals," *Journal of Zoology*, vol. 186, no. 1, pp. 61–81, 1978.

[11] R. M. Alexander, "Optimum walking techniques for quadrupeds and bipeds," *Journal of Zoology*, vol. 192, no. 1, pp. 97–117, 1980.

[12] T. M. Griffin, R. P. Main, and C. T. Farley, "Biomechanics of quadrupedal walking: how do four-legged animals achieve inverted pendulum-like movements?" *Journal of Experimental Biology*, vol. 207, no. 20, pp. 3545–3558, 2004.

[13] T. McGeer, "Passive dynamic walking," *The International Journal of Robotics Research*, vol. 9, no. 2, pp. 62–82, 1990.

[14] F. Asano, M. Yamakita, and K. Furuta, "Virtual passive dynamic walking and energy-based control laws," in *2000 IEEE/RSJ International Conference on Intelligent Robots and Systems (IROS)*, vol. 2, 2000, pp. 1149–1154.

[15] Z. Gan and C. D. Remy, "A passive dynamic quadruped that moves in a large variety of gaits," in *2014 IEEE/RSJ International Conference on Intelligent Robots and Systems*, 2014, pp. 4876–4881.